Excited-state symmetry breaking in solvent mixtures

Balanikas, Vangelis; Reymond-Joubin, Maric; Vauthey, Eric

How to cite

BALANIKAS, Vangelis, REYMOND-JOUBIN, Maric, VAUTHEY, Eric. Excited-state symmetry breaking in solvent mixtures. In: The journal of physical chemistry letters, 2024, vol. 15, n° 9, p. 2447–2452. doi: 10.1021/acs.jpclett.4c00213

This publication URL: https://archive-ouverte.unige.ch/unige:175483
Publication DOI: 10.1021/acs.jpclett.4c00213

Photoinduced Electron Transfer between Dipolar Reactants: Solvent and Excitation-Wavelength Effects

Pragya Verma, Darya S. Budkina, and Eric Vauthey*

Department of Physical Chemistry, University of Geneva, 30 Quai Ernest-Ansermet, 1211 Geneva, Switzerland

E-mail: eric.vauthey@unige.ch

Abstract

Electron transfer (ET) quenching in non-polar media is not as well understood as in polar environments. Here, we investigate the effect of dipole-dipole interactions between the reactants using ultrafast broadband electronic spectroscopy combined with molecular dynamics simulations. We find that the quenching of the S_1 state of two polar dyes, coumarin 152a and Nile red, by the polar N,N-dimethylaniline (DMA) in cyclohexane is faster by a factor up to 3 when exciting on the red edge rather than at the maximum of their $S_1 \leftarrow S_0$ absorption band. This originates from the inhomogeneous broadening of the band due to a distribution of the number of quencher molecules around the dyes. As a consequence, red-edge excitation photoselects dyes in a DMA-rich environment. Such broadening is not present in acetonitrile and no excitation wavelength dependence of the ET dynamics is observed. The quenching of both dyes is markedly faster in non-polar than polar solvents, independently of the excitation wavelength. According to molecular dynamics simulations, this is due to the preferential solvation of the dyes by DMA in cyclohexane. The opposite preferential solvation is predicted in acetonitrile. Consequently, close contact between the reactants requires partial desolvation. By contrast, the recombination of the quenching product is slower in non-polar than in polar solvents and exhibit much smaller dependence, if any, on the excitation wavelength.

Introduction

Bimolecular photoinduced electron transfer (ET) reactions have been thoroughly investigated both experimentally and theoretically in polar environments.[1–11] Comparatively, these processes have been much less studied in non-polar media. One reason for this is that one of the main applications of these reactions is the production of free ions, a process that requires a sufficiently polar environment to ensure the dissociation of the ion pairs.[12] However, other applications, such as organic photovoltaics,[13–15] also rely on intermolecular photoinduced ET, which has to occur in a rigid environment of relatively low polarity.

ET reactions are generally assumed to be much less efficient in non-polar solvents, mainly because of the smaller driving force.[16–18] Indeed, intramolecular photoinduced ET in donor-bridge-acceptor systems with a fixed distance between the electron donor and acceptor is not often observed in apolar solvents. By contrast, the relatively few of ET quenching studies in non-polar solvents revealed that this process can be diffusion controlled.[19,20] Investigations of the early dynamics using models which take the time dependence of the quenching rate into account found that the intrinsic

ET rate constant in non-polar solvents was as large or even larger than in polar ones.[21–24] These high intrinsic quenching rates, independently of the solvent polarity, were explained by the large electronic coupling that can be achieved in the reactant pair, making ET an adiabatic process. Consequently, the quenching product is a highly coupled ion pair, that can also be viewed as an exciplex.[7,24] Additionally, the contribution of the static quenching to the overall fluorescence quenching of cyanoanthracene derivatives by aromatic electron donors was found to be significantly larger in cyclohexane than in acetonitrile.[24] This was tentatively explained in terms of preferential solvation of the fluorophores by the donors via dispersion interactions. Whereas specific interactions, such as hydrogen-bonding, have been shown to significantly influence the dynamics of intermolecular photoinduced reactions,[25–31] much less is known about the effect of non-specific interactions.

Here, we explore the influence of preferential solvation on the ET quenching dynamics, concentrating on the effect of dipole-dipole interactions between the reactants. We selected coumarin 152a (C152a) and Nile red (NR), which are polar in the ground state and exhibit a large absorption solvatochromism,[32–34] as fluorophores, and N,N-dimethylaniline (DMA) as polar donor. Photoinduced ET with the C152a/DMA pair in non-polar solvents was previously investigated using femtosecond fluorescence up-conversion.[35] The quenching dynamics were found to be significantly faster upon red-edge excitation than upon irradiation at the band maximum of the fluorophore. This was explained in terms of a inhomogeneous broadening of the $S_1 \leftarrow S_0$ absorption band of C152a in the presence of DMA, i.e. by considering that dyes with nearby DMA molecules are better solvated than those with only apolar solvent around and, thus, absorb at longer wavelength. Here, we investigate this excitation wavelength dependence further using broadband fluorescence up-conversion (FLUPS) as well as electronic transient absorption (TA) spectroscopies. We show that not only the fluorescence dynamics but also the emission spectrum depend on the excitation wavelength, confirming the inhomogeneous nature of the absorption spectrum and the possibility to photoselect fluorophores with different environments. We also investigate whether this photoselection influence the dynamics of the ensuing quenching product. Our results reveal that, although the ionic product is generated faster upon red-edge excitation, its decay by charge recombination exhibit only a weak, if present, excitation wavelength dependence. Finally, we show that fluorescence quenching of both fluorophores by DMA is considerably faster in cyclohexane than in acetonitrile. On the basis of molecular dynamics simulations, we explain this unexpected solvent dependence by the preferential solvation of the fluorophore by polar donors, which takes place in cyclohexane but not in acetonitrile.

Methods

Sample

The fluorophores, coumarin 152A (C152, Exciton) and Nile red (NR, Sigma-Aldrich) were used as received. The solvents, cyclohexane (CHX, Acros Organics), tetrahydrofuran (THF, Carl Roth) and acetonitrile (ACN, Acros Organics) were of spectroscopic grade and used without further purification. N, N-dimethylaniline (DMA, Aldrich) was vacuum distilled and kept in the dark under argon.

Stationary spectroscopy

Stationary electronic absorption spectra were measured with a Cary50 spectrometer. Stationary fluorescence spectra were recorded with a Horiba FluoroMax-4 spectrofluorometer and were subsequently corrected with a set of secondary emissive standards.[36]

Time-resolved spectroscopy

Broadband fluorescence up-conversion spectroscopy (FLUPS) measurements were carried out with a setup described in ref. 37, based on the design of Ernsting and coworkers.[38] The pump pulses were either at 400 or

425 nm. In the first case, the pulses were produced by frequency doubling part of the output of a Ti:Sapphire amplifier system (Spectra-Physics, Solstice Ace, 30 fs, 800 nm, 5 kHz). The pump pulses at 425 nm were generated with a TOPAS-Prime combined with a NirUVis module (LightConversion). The gate pulses at 1340 nm were produced with an optical parametric amplifier (TOPAS C, Light Conversion) pumped at 800 nm. The polarization of the pump pulses was at magic angle relative to that of the detected fluorescence. The full width at half maximum (FWHM) of instrument response function (IRF), estimated from the Raman signal of the solvent, was less than 100 fs. Photometric correction of the emission spectra was carried using secondary standards. The chirp was corrected using the prompt rise of the fluorescence of BBOT solutions. The absorbance of the samples at the excitation wavelength did not exceed 0.2 in a 1 mm quartz cuvette. The FLUPS spectra were corrected for the reabsorption.

Electronic transient absorption (TA) measurements were performed using a setup described in ref. 39,40 and based on the same amplified Ti:Sapphire system as above. Pump pulses at 400 nm were produced by frequency doubling part of the 800 nm amplifier output. Pulses at other wavelengths were generated using a TOPAS-Prime combined with a NirUVis module (Light Conversion), and were compressed to 60–100 fs at the sample position. The pump intensity on the sample was $\sim$0.15–0.75 mJ/cm^2. Probing was achieved from about 350 to 750 nm using white light pulses produced in a 3 mm CaF_2 plate. The polarisation of the pump pulses was at magic angle with respect to that of the probe pulses. The sample cell was 1 mm thick and the FWHM of the IRF varied between 80 and 350 fs, depending on the probe wavelength.

Molecular dynamics simulations

Molecular dynamics (MD) simulations were carried out using GROMACS 2023.1.[41] The OPLS-AA force field was used for the solvents as well as for the solute nonbonded parameters.[42,43] The topology files of the fluorophores and DMA, were generated using the Antechamber Python parser interface (ACPYPE) tool,[44] with as input the optimised structures obtained from DFT quantum-chemical calculations (B3LYP/6-31G+d)[45] as implemented in the Gaussian 16 package.[46] The atomic charges were determined from CHELPG fits of the electrostatic potential obtained from the DFT calculations.[47] A periodic cubic box (5x5x5 nm^3) was used for the simulations, which were performed at constant pressure (1 atm)[48] and temperature (295 K)[49] with 2 fs steps for 50 ns. Further details on the simulation parameters can be found in the SI (section S4).

Results

Stationary spectroscopy

As illustrated in Figure 1, the $S_1 \leftarrow S_0$ absorption band of both C152a and NR in CHX shows enhanced intensity on its red side upon addition of DMA as well as a less pronounced vibronic structure. By contrast, addition of DMA does not affect the spectra in THF and ACN (Figures S1 and S2). This effect, already observed previously with C152a,[35] is assigned to an inhomogeneous broadening of the $S_1 \leftarrow S_0$ band due to the presence of dye populations with different amounts of polar DMA in the vicinity and, hence, different $S_1 \leftarrow S_0$ transition energies, as expected from the strong absorption solvatochromism of C152a and NR.[32,33] In CHX, the presence of a DMA near a polar dye leads to a significant increase in the solvation energy. This is no longer the case in THF and ACN, where the presence of DMA near a dye molecule does not significantly change the solvation energy.

Absorption of donor-acceptor complexes as the origin of the spectral broadening can be excluded for at least two reasons. First, the broadening is only present in non-polar solvents, whereas donor-acceptor complex formation do not exhibit such solvent dependence. Second, excitation in the charge-transfer band of these complexes leads to the direct population of an ion-pair state,[4,50] whereas, as shown

below, red-edge excitation of C152a and NR with DMA populates the S_1 state of the chromophore.

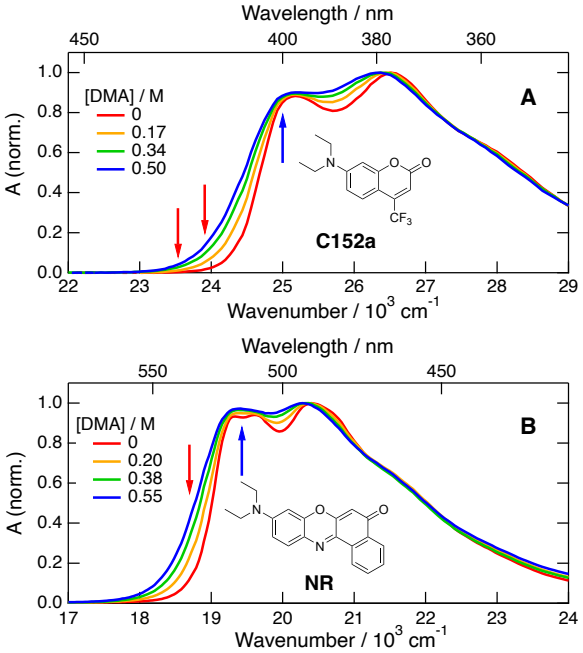

Figure 1: Stationary electronic absorption spectra recorded with (A) C152a and (B) NR in cyclohexane and different concentrations of DMA. The arrows represent the excitation wavelengths.

Quenching dynamics

The above results suggest that red-edge excitation of C152a and NR in CHX should lead to a photoselection of dyes in a more polar environment than pure CHX. To have a better insight into these local environments, we performed FLUPS measurements with C152a upon red-edge excitation at 425 nm and excitation at 400 nm, near the band maximum (Figure 1). As depicted in Figure 2, the transient emission band upon red-edge excitation is red shifted by about -1000 cm^{-1} relatively to that measured upon 400 nm excitation. For a given excitation wavelength, the transient spectra do not exhibit any temporal shift during the fluorescence lifetime.

The red shift of the transient spectra can be better appreciated by comparing the FLUPS spectra with the stationary spectra measured

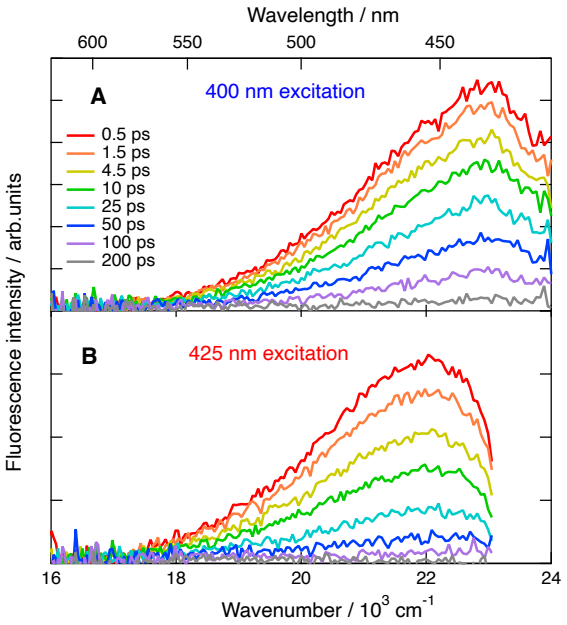

Figure 2: Transient emission spectra recorded at various time delays after (A) band-maximum and (B) red-edge excitation of C152a in cyclohexane with 0.5 DMA.

in CHX and THF without DMA (Figure 3). The transient spectra with DMA upon red-edge excitation are approximately located between those in pure CHX and THF. Comparatively, those recorded upon 400 nm excitation are closer to the stationary spectrum in CHX. These shifts are less pronounced with 0.4 instead of 0.5 M DMA (Figure S3). These FLUPS spectra confirm that dyes in more polar environments can be photoselected upon red-edge excitation. The position of the FLUPS spectra with 0.5 M DMA upon red-edge excitation is between those reported for this dye in butyl- and diethyl-ether,[51] which have a static dielectric constant, ϵ_s, of 3.1 and 4.3, respectively. These ϵ_s values should compared with those of 2.0 and 4.4 for CHX and DMA.

In agreement with the previous investigation,[35] the fluorescence quenching dynamics of C152a in CHX are strongly accelerated upon red-edge excitation (Figure 4). The quenching dynamics could be reproduced by the convolution of the IRF with a sum of three exponential functions. As the resulting time constants have no physical meaning, we use the amplitude-averaged lifetime, τ_{av}, as well as the time after

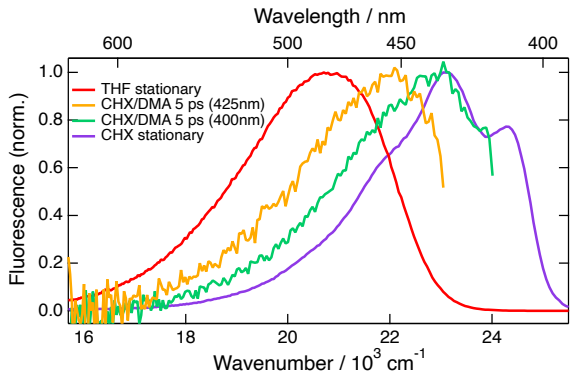

Figure 3: Comparison of the transient emission spectra recorded upon red-edge and band-maximum excitation of C152a with 0.5 M DMA in cyclohexane with stationary emission spectra in cyclohexane and tetrahydrofuran.

which the fluorescence intensity has decayed by a factor e, τ_e, to discuss the effect of the excitation wavelength (Table S1). We also define an 'acceleration factor' F as $F = \tau_e^{\max}/\tau_e^{\mathrm{re}}$, where $\tau_e^{\max}$ and τ_e^{re} are the τ_e values upon band maximum and red-edge excitation, respectively. At 0.5 M DMA, τ_e decreases from 40 to 15 ps corresponding to an acceleration factor of $F = 2.7$.

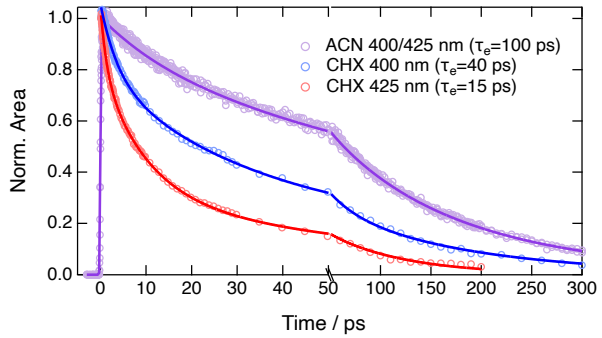

Figure 4: Time profiles of the fluorescence band area recorded after 400 and 425 nm excitation of C152a with 0.5 M DMA in cyclohexane and acetonitrile, and best multiexponential fits.

In the polar THF and ACN, the FLUPS spectra recorded with 0.5 M DMA are at similar position than the corresponding stationary emission spectra without quencher (Figure S4). Contrary to CHX, no excitation wavelength dependence of the quenching dynamics was observed (Figure S5). Surprisingly, the overall quenching dynamics at the same quencher concentration are significantly slower than in CHX, with τ_e amounting to 170 and 100 ps in THF and ACN, respectively (Figure 4, Table S1). The same difference between CHX and ACN can be observed when looking at the fastest decay component, which can be considered as that associated with the static limit of the quenching. On the other hand, the fastest quenching component in THF is similar to that in CHX but its relative amplitude is considerably smaller.

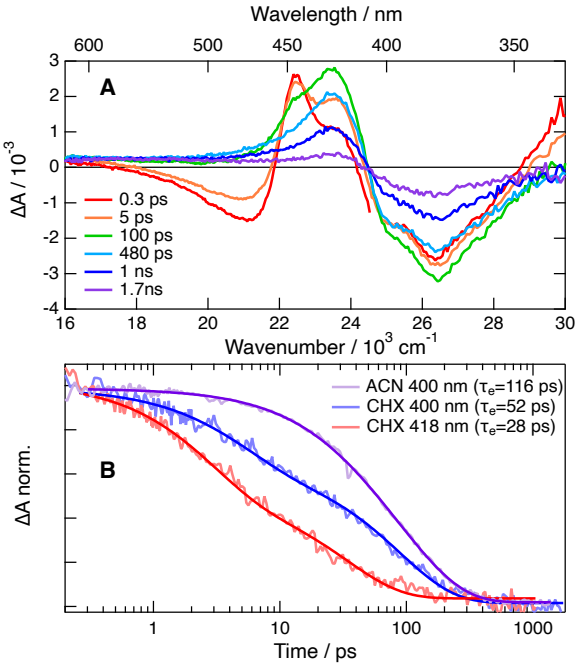

Figure 5: A) Transient absorption spectra recorded at various times after 400 nm excitation of C152a in cyclohexane with 0.5 M DMA and B) time dependence of the transient absorption due to C152a in the S_1 state in cyclohexane upon 400 and 418 nm excitation and in acetonitrile upon 400 nm excitation and best multiexponential fits.

The quenching dynamics were also investigated by TA spectroscopy upon 400 and 418 nm excitation. The early TA spectra are similar to those recorded without DMA (Figures 5A and S6). They are dominated by an excited-state absorption (ESA) band around 450 nm that can be assigned to a $S_{n>1} \leftarrow S_1$ transition as well as by negative bands that originate from stimulated emission (SE) and ground-state bleach

(GSB). Both the ESA and SE bands decay on a timescale that depends on quencher concentration and a new positive band at 425 nm rises concurrently (Figure 5A). The same band is observed when using 1,2,4-trimethoxybenzene instead of DMA as electron donor (Figure S7A). Consequently, it is assigned to the radical anion of the dye, C152a$^{\bullet-}$. The radical cation DMA$^{\bullet+}$ also absorbs in this region, but its absorption coefficient is probably too small relatively to that of C152a$^{\bullet-}$ to make this species visible.[52,53] These data could be well reproduced by global analysis assuming a series of three successive steps, $A \rightarrow B \rightarrow C \rightarrow$.[54,55] The resulting evolution-associated difference spectra and time constants are shown in Figure S8.

Insight into the effect of the excitation wavelength on the quenching dynamics was obtained by looking at the time evolution of C152a*. Figure 5 indicates that C152a* has no transient absorption around 455 nm, so that the TA profile at that wavelength reflects the time evolution of C152a$^{\bullet-}$. The time evolution of C152a* was obtained by subtracting the TA profile of C152a$^{\bullet-}$ after proper intensity correction from that measured at the ESA band maximum around 450 nm, which is due to both C152a* and C152a$^{\bullet-}$. As illustrated in Figure 5B and S9, the quenching dynamics with 0.2, 0.4 and 0.5 M DMA are significantly faster upon 418 than 400 nm excitation with acceleration factors F of 1.75, 3 and 2, respectively. Such excitation wavelength dependence was not observed in ACN, in agreement with the FLUPS measurements. Figure 5B also reveals that the quenching dynamics in CHX are more than twice as fast as in ACN, independently of the excitation wavelength.

To check the generality of the excitation wavelength dependence in CHX and of the faster quenching than in ACN, similar TA measurements were performed with NR upon red edge excitation at 535 nm, and excitation at 510 nm around the maximum of the $S_1 \leftarrow S_0$ band. As depicted in Figure 6, the early TA spectra are dominated by the negative SE and GSB bands in the 650 and 500 nm regions as well as positive ESA bands peaking around 460 and 350 nm. These spectra are identical to those measured without DMA (Figure S12) and can thus be assigned to the NR in the S_1 state, NR*. These spectra transform on a timescale that depends on the DMA concentration into a spectrum consisting of the GSB band surrounded by two broad positive bands. These features are assigned to the radical anion of the dye, NR$^{\bullet-}$, with a possible contribution of DMA$^{\bullet+}$.

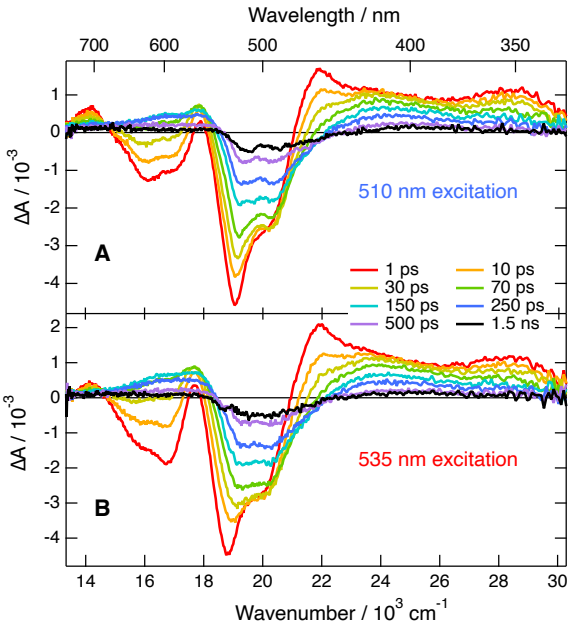

Figure 6: Transient absorption spectra recorded at various times after band-maximum (A) and red-edge (B) excitation of NR in cyclohexane with 0.5 M DMA.

Interestingly, the shape of the SE band depends markedly on both the DMA concentration and the excitation wavelength (Figures 6 and S12). At low DMA concentration, the SE band has a maximum at about 620 nm with a shoulder at 575 nm. As the quencher concentration rises, the relative intensity of these two features changes and the shoulder becomes dominant. At a given DMA concentration, the shoulder is systematically more intense upon red-edge than band-maximum excitation. For example, the shape of the SE band with 510 nm excitation and 0.55 M DMA is the same as with red-edge excitation and 0.2 M DMA (Figure S12). This dependence of the SE on the excitation wavelength is a clear indication that dyes with different environments are photoselected,

like with C152a. Moreover, these data reveal that with a bulk DMA concentration of 0.2 M, red-edge excitation selects dyes with a much larger local DMA concentration. Consequently, a strong excitation wavelength dependence of the quenching dynamics can be expected.

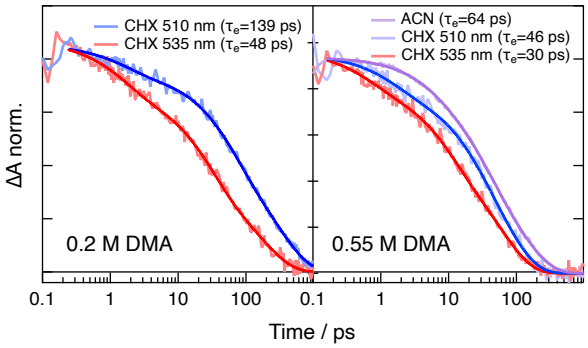

Figure 7: Time dependence of the transient absorption due to NR in the S_1 state in cyclohexane upon band-maximum and red-edge excitation and in acetonitrile upon 535 nm excitation with different DMA concentrations and best multiexponential fits.

Like those with C152a, these data could be well reproduced by global analysis assuming a series of three successive steps (Figure S13). The quenching dynamics were determined from the time evolution of the TA at 452 nm, where the ionic product has no contribution to the transient absorption. As expected, quenching is significantly faster upon red-edge than band-maximum excitation (Figure 7) with an acceleration factors F decreasing from 2.9 to 1.5 by increasing DMA concentration from 0.2 to 0.55 M. This dependence of F on the quencher concentration is qualitatively similar to that found with C152a. Incidently, the quenching dynamics measured with 0.2 M DMA upon red-edge excitation are very similar to that recorded with 0.55 M DMA upon excitation at the band maximum (Figure 7). This is a further support of the DMA-rich environment of the dyes photoselected upon red-edge excitation. In this case again, the ET quenching dynamics of NR are faster in CHX than in ACN, independently of the excitation wavelength (Figures 7 and S14).

Recombination dynamics

We now consider whether the different environments that can be photoselected have an influence on the fate of the quenching product, i.e. on the charge recombination (CR) dynamics. The time evolution of $C152a^{\bullet-}$ was obtained from the TA profile around 455 nm, where C152a* has no contribution to the signal. For $NR^{\bullet-}$, we took the TA profiles around 405 nm where this species absorbs predominantly and subtracted the TA profile at 452 nm due to NR* only after proper intensity correction.

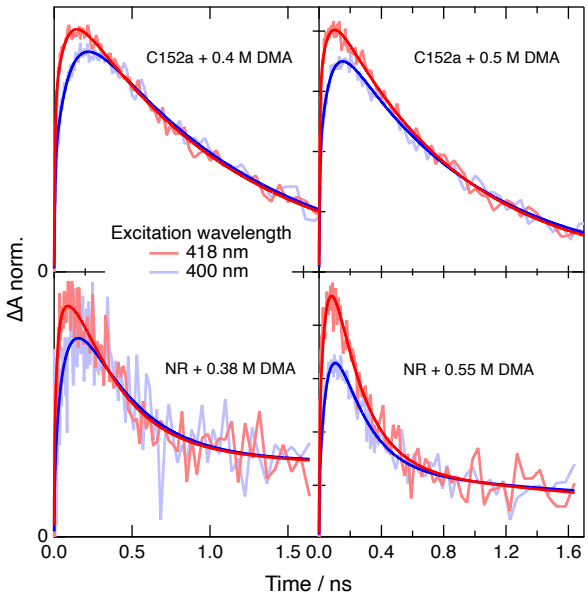

Figure 8: Time profiles of the ionic product resulting from the quenching of C152a and NR by DMA in cyclohexane and best fits of eq.(1).

The resulting time evolutions of $C152a^{\bullet-}$ and $NR^{\bullet-}$ in CHX are depicted in Figure 8. As expected from the quenching dynamics, the build up of the ion signal is significantly faster upon red-edge than band-maximum excitation for both dyes. However, the decay of the signal is apparently independent of the excitation wavelength. To have more quantitative insight into the CR dynamics, the time profiles of the ion signal, $\Delta A_{\mathrm{ion}}(t)$, were analysed using the following equation:[56]

$$\Delta A_{\mathrm{ion}}(t) = C \cdot \int_0^t P_{\mathrm{ion}}(t-t') \cdot \dot{P}_{\mathrm{S1}}(t')\,\mathrm{d}t', \quad (1)$$

where C is an adjustable normalisation constant, $P_{\mathrm{ion}}(t)$ is the intrinsic recombination dynamics that would be observed if the ions were generated instantaneously and $\dot{P}_{\mathrm{S1}}(t)$ is the time-derivative of the quenching dynamics, representing the rate of ion formation. In the analysis, the time derivative of the best multiexponential fit of the quenching dynamics was taken as $\dot{P}_{\mathrm{S1}}(t)$ and was kept constant. $P_{\mathrm{ion}}(t)$ was described as a sum of exponential functions with adjustable amplitudes and time constants. For both dyes and all DMA concentrations, the sum of two exponential functions was sufficient to properly reproduce the data with the best-fit parameters given in Table 1. The biexponential nature of the CR dynamics can be interpreted as a distribution of rate constants, that itself originates from a distribution of ion pairs with different mutual orientations and environments.[11,57,58]

Table 1: Time constants, τ_i, and relative amplitudes, A_i (A_2=1-A_1), obtained from the fit of eq.(1) to the data shown in Figure 8.

Dye	[DMA] / M	λ_{ex} / nm	τ_1 / ps	A_1	τ_2 / ns
C152a	0.2	400	177	0.35	∼2.1
C152a	0.2	418	103	0.42	∼1.6
C152a	0.4	400	94	0.30	∼1.1
C152a	0.4	418	69	0.20	∼1.1
C152a	0.5	400	92	0.20	0.89
C152a	0.5	418	40	0.15	0.82
NR	0.38	510	360	0.73	> 2
NR	0.38	535	305	0.74	> 2
NR	0.55	510	200	0.79	> 2
NR	0.55	535	190	0.74	> 2

Overall, both CR time constants decrease with increasing DMA concentration. This effect can be explained by the associated polarity increase of the environment. Indeed, contrary to the quenching dynamics, CR is significantly faster in ACN than in CHX. As illustrated in Figures S10 and S14, no ion signal is visible in the TA spectra recorded with both dyes and DMA in ACN, pointing to CR occurring on a much shorter timescale than quenching. Furthermore, the CR dynamics measured with C152a in pure DMA can be reproduced using a single exponential function with a CR time constant of 77 ps (Figure S11). Such faster CR in polar environments can be explained by a reduction of the driving force due to the stabilisation of the ionic product by solvation.[59] As CR occurs in the Marcus inverted region, it accelerates upon decreasing the driving force.[50,60,61]

The shorter CR time constant is apparently systematically smaller upon red-edge than band-maximum excitation (Table 1). Although this difference should be considered with caution given the relatively large uncertainty on these time constants ($\sim \pm 25\%$), it is consistent with the polarity dependence discussed just above. Indeed, red-edge excitation photoselects dyes in a DMA-rich environment, which is more polar than that of dyes excited in the band maximum. Consequently, the resulting ion pairs should be stabilised relatively to those produced upon shorter wavelength excitation and should, thus, recombine faster. However, even if this latter effect is really present, the excitation wavelength dependence of CR is markedly smaller than that observed for the quenching.

Discussion

Whereas differences in local polarity could explain the excitation wavelength dependence of CR, if present, they cannot account for the much larger one observed with the quenching dynamics. Although the DMA concentration around a dye affects the local polarity, it especially determines the number of quenching pathways of the excited state. As illustrated in Figure 9, the quenching rate constant is given by:[62,63]

$$k_{\mathrm{q}} = \sum_{i=1}^{n} k_{\mathrm{CS},i}, \qquad (2)$$

where $k_{\mathrm{CS},i}$ is the rate constant of charge separation (CS) between the excited dye and one of the n surrounding quencher molecules. Therefore, molecules excited on the red-edge undergo faster quenching because of the larger n. On the other hand, CR is a two-body process (Figure

9) and its dynamics do not depend on n, apart from the possible influence of the local polarity.

Extracting the individual CS rate constants, $k_{CS,i}$, from the quenching dynamics is not really possible because quenching depends on the overall electronic coupling, rather than simply on n. This coupling could be larger with a single DMA at optimal distance/orientation than with several quenchers with less favourable distance/orientation.

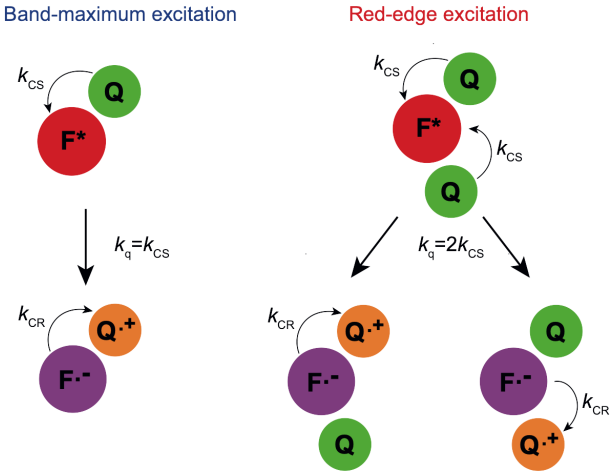

Figure 9: Schematic illustration of the differences in the excitation-wavelength dependence of the ET quenching and charge recombination dynamics (F: fluorophore; Q: quencher).

The above results with both dyes reveal that the excitation wavelength-dependence of the quenching dynamics tends to decrease above a certain DMA concentration. This originates from the fact that the extent of inhomogeneous broadening of the $S_1 \leftarrow S_0$ absorption band of the dye depends on the diversity of the local environments. At high quencher concentration, all dyes are surrounded by several quenchers. They have, thus, similarly polar environments and experience similar solvatochromism.

To have a better insight into the distribution of local environments at a given quencher concentration, we performed MD simulations of 5x5x5 nm^3 boxes filled with CHX and containing one C152a and 10, 20 or 40 molecules of DMA, corresponding to quencher concentrations of 0.17, 0.34 and 0.68 M (see Section S4 for details). These boxes were simulated for 50 ns and the minimum interatomic distance between C152a and each DMA was determined. Figure 10 presents histograms of the number of DMA in contact with C152a, i.e. at an interatomic distance of $\leq$0.3 nm, at different quencher concentrations, whereas snapshots from the simulations are shown in Figure S16. These histograms suggest that, whereas at the lowest concentration, the majority of dye molecules do not have a DMA at contact distance, more than 90% of them are in contact with at least one DMA at the highest concentration. In the latter case, more than half of the dyes have two or more DMA in their close vicinity. This implies that, even upon band-maximum excitation, most dyes should undergo ultrafast static quenching. In this case, ET upon red-edge excitation should still be faster but with a smaller acceleration factor F than at 0.17 M DMA, where quenching upon band-maximum excitation should require some diffusion and thus be significantly slower.

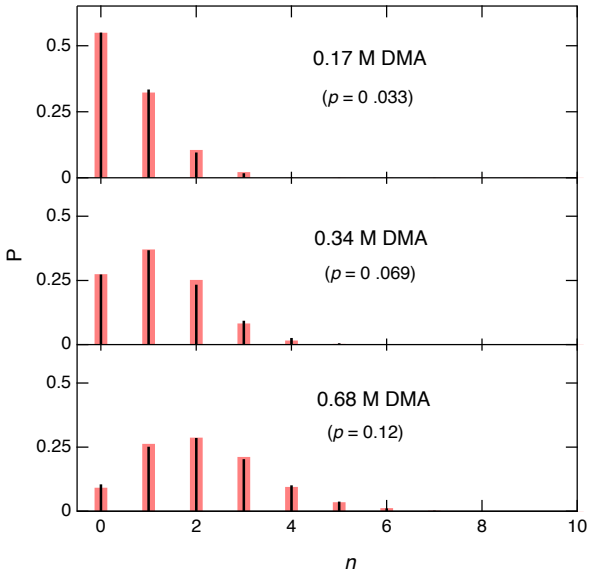

Figure 10: Histograms of n, the number of DMA in contact with C152a, obtained from MD simulations (red) and best fits of eq.3 with $N = 18$ (black)).

These histograms were analysed using the binomial distribution:[64]

$$f_{N,p}(n) = \frac{N!}{(N-n)!n!} p^n (1-p)^{N-n}, \quad (3)$$

where N is the number of sites around the solute, n the number of DMA molecules in contact and p the probability for a molecule to be a DMA rather than a solvent. A value of $N = 18$, estimated from the simulations, was used and the only adjustable parameter was p. As shown in Figure 10, the value of p, obtained from such analysis, is proportional to the quencher concentration, as expected. However, the model is too crude to interpret the absolute value of this parameter.

To find out whether these distributions of DMA around C152a in CHX are influenced by solute-solvent interactions, the MD simulations were repeated with 0.34 M isopropylcyclohexane (IPC) and isopropylbenzene (IPB) as co-solutes instead of DMA. Both IPC and IPB are similar in shape and volume to DMA, but have negligible permanent dipole moment. Comparison of IPC and IPB allows for an estimation of the effect of dispersion interactions. The histograms of the number of IPC and IPB in contact with C152a reveal marked difference with that obtained with DMA at the same concentration (Figure 11): about 50% of the dyes have no IPC or IPB at contact vs. less than 30% with DMA (Figure 10). This difference is also reflected by the parameter p obtained from the fit of eq.3, which is around 0.04 for IPC and IPB, but significantly larger, around 0.07, with DMA. These results suggest that dipole-dipole interactions enhances the local DMA concentration around the polar dyes, and thus, results in a local dielectric enrichment. On the other hand, only small differences can be observed between IPC and IPB (Figure 11A,B), pointing to a minor role of dispersion interactions in the preferential solvation. However, as induced polarisation is not accounted for in these MD simulations, the effect of dispersion could be underestimated.[65]

Finally, the simulations were repeated with DMA in ACN to find out whether preferential solvation by DMA is also predicted in a highly polar environment. The histograms of the number of DMA in contact (Figure 11C) point to a markedly smaller local quencher concentration around C152a in ACN than in CHX, p being equal to 0.026 vs 0.069. This can be

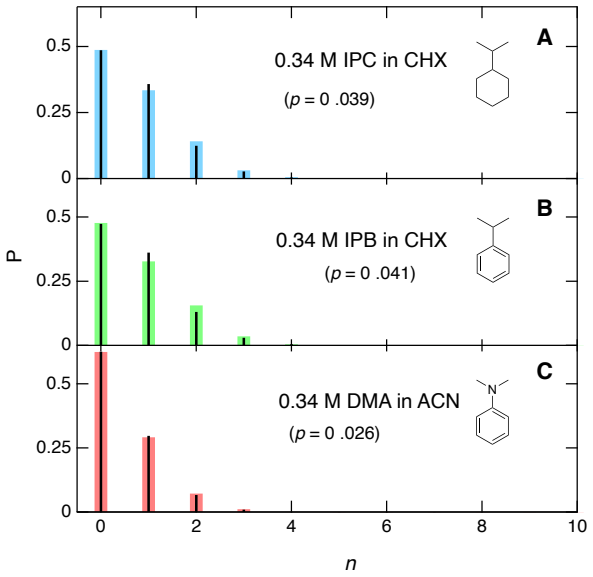

Figure 11: Histograms of n, the number of co-solutes in contact with C152a in CHX (A,B) and in ACN (C), obtained from MD simulations (thick bars) and best fits of eq.3 with $N = 18$ (black)).

easily explained by considering that the dipole-dipole interactions with ACN are stronger than with DMA, due to the larger dipole moment (3.44 vs. 1.6 D) and smaller size of ACN, resulting in a larger solvation energy with ACN. Consequently, the preferential solvation is now in favour of ACN. This suggests that, whereas close contact between the dye and DMA is favoured in non-polar solvents, it requires partial desolvation in ACN. This leads to a smaller electronic coupling in ACN compared to that in CHX and thus to slower quenching, as observed experimentally. Because of this larger electronic coupling in non-polar environments, ET can, most probably, no longer be considered as a non-adiabatic process, as already hinted by previous investigations.[7,24,66–68] In this case, ET quenching should rather be viewed as a non-radiative transition to a charge-transfer state taking place in a supermolecule, comprising the dye and one or more quenchers.

Conclusions

The results described here reveal that dipole-dipole interactions between the reactants have

a strong effect on the dynamics of bimolecular photoinduced ET reactions in non-polar environments. These interactions favour close contact between the reactants and, if one reaction partners is more concentrated, as it is normally the case in ET quenching experiments, preferential solvation of the chromophore by quenchers. By contrast, polar reactants in polar solvents are preferentially surrounded by solvent molecules. Consequently, close contact between the reactants requires partial desolvation and is thus less favourable than in non-polar media. This difference has a strong impact on the electronic coupling and thus on the ET rate. For this reason, ET quenching in non-polar environments occurs mostly in the static limit and is markedly faster than in polar media, contrary to expectations based on energetics considerations.

Another consequence of the preferential solvation by the quencher in non-polar media is that the absorption solvatochromism of the chromophore is correlated with the number of surrounding quencher molecules. This leads to an inhomogeneous broadening of the absorption band and opens the possibility to photoselect dyes with different local quencher concentrations by tuning the excitation wavelength. Because of this, the ET quenching dynamics in non-polar solvents depend strongly on the excitation wavelength contrary to the polar solvents where such inhomogeneous broadening mechanism is absent. Although the contribution of dispersion interactions to the preferential solvation by the quencher could not be evidenced here by the simulations, it can be expected to be significant with dyes that are more soluble in liquid aromatic quenchers than in non-polar solvents like CHX. These effects, which should also be present in solid and weakly polar media like those used in organic photovoltaics, certainly deserve further scrutinising.

Acknowledgement The authors thanks the Swiss National Science Foundation (grant 200020-184607) and the University of Geneva are thanked for their financial support. The computations were performed at University of Geneva using Baobab HPC service.

Supporting Information Available

Stationary spectra, transient emission and absorption spectra, MD simulations. All data can be downloaded from https://doi.org/10.26037/yareta:vo4jtzixorg2jm pw2r2syq3tc4.

References

(1) Weller, A. Exciplex and Radical Pairs in Photochemical Electron Transfer. *Pure Appl. Chem.* **1982**, *54*, 1885–1888.

(2) Gould, I. R.; Farid, S. Dynamics of Bimolecular Photoinduced Electron Transfer Reactions. *Acc. Chem. Res.* **1996**, *29*, 522–528.

(3) Kakitani, T.; Matsuda, N.; Yoshimori, A.; Mataga, N. Present and Future Perspectives of Theoretical Aspect of Photoinduced Charge Separation and Charge Recombination Reactions in Solution. *Prog. Reaction Kinetics* **1995**, *20*, 347–381.

(4) Mataga, N.; Miyasaka, H. Electron Transfer and Exciplex Chemistry. *Adv. Chem. Phys.* **1999**, *107*, 431–496.

(5) Burshtein, A. Unified Theory of Photochemical Charge Separation. *Adv. Chem. Phys.* **2000**, *114*, 419–587.

(6) Balzani, V. *Electron Transfer in Chemistry*; J. Wiley: New York, 2001.

(7) Murata, S.; Tachiya, M. Unified Interpretation of Exciplex Formation and Marcus Electron Transfer on the Basis of Two-Dimensional Free Energy Surfaces. *J. Phys. Chem. A* **2007**, *111*, 9240–9248.

(8) Rosokha, S. V.; Kochi, J. K. Fresh Look at Electron-Transfer Mechanisms via the Donor/Acceptor Bindings in the Critical Encounter Complex. *Acc. Chem. Res.* **2008**, *41*, 641–653.

(9) Rosspeintner, A.; Vauthey, E. Bimolecular Photoinduced Electron Transfer Reactions in Liquids under the Gaze of Ultrafast Spectroscopy. *Phys. Chem. Chem. Phys.* **2014**, *16*, 25741–25754.

(10) Angulo, G.; Rosspeintner, A. Bimolecular Photo-Induced Electron Transfer Enlightened by Diffusion. *J. Chem. Phys.* **2020**, *153*, 040902.

(11) Vauthey, E. Elucidating the Mechanism of Bimolecular Photoinduced Electron Transfer Reactions. *J. Phys. Chem. B* **2022**, *126*, 778–788.

(12) Fuoss, R. M. Ionic Association. III. The Equilibrium between Ion Pairs and Free Ions. *J. Am. Chem. Soc.* **1958**, *80*, 5059–5061.

(13) Clarke, T. M.; Durrant, J. R. Charge Photogeneration in Organic Solar Cells. *Chem. Rev.* **2010**, *110*, 6736–6767.

(14) Heeger, A. J. 25th Anniversary Article: Bulk Heterojunction Solar Cells: Understanding the Mechanism of Operation. *Adv. Mater.* **2014**, *26*, 10–28.

(15) Ingannäs, O. Organic Photovoltaics over Three Decades. *Adv. Mater.* **2018**, *30*, 1800388.

(16) Oevering, H.; Paddon-Row, M.; Heppener, M.; Oliver, A.; Cotsaris, E.; Verhoeven, J.; Hush., N. Long-Range Photoinduced Through-Bond Electron Transfer and Radiative Recombination via Rigid Non-Conjugated Bridges: Distance and Solvent Dependence. *J. Am. Chem. Soc.* **1987**, *109*, 3258–3269.

(17) Heitele, H.; Pöllinger, F.; Weeren, S.; Michel-Beyerle, M. E. Influence of Solvent Polarity on Intramolecular Electron Transfer. A Consistency Test of Free Energies of Reaction and Solvent Reorganization with Experimental Rates. *Chem. Phys.* **1990**, *143*, 325–332.

(18) Kuciauskas, D.; Liddell, P. A.; Lin, S.; Stone, S. G.; Moore, A. L.; Moore, T. A.; Gust, D. Photoinduced Electron Transfer in Carotenoporphyrin-Fullerene Triads: Temperature and Solvent Effects. *J. Phys. Chem. B* **2000**, *104*, 4307–4321.

(19) Abdullah, K.; Kemp, T. Electron Donor-Acceptor Quenching of the Fluorescence of 9-10 Dicyanoanthracene in Polar and Non-Polar Solvents. *J. Photochem.* **1983**, *28*, 61.

(20) Chen, J. M.; Ho, T. I.; Mou, C. Y. Experimental Investigation of Excited-State Electron-Transfer Reaction: Effects of Free Energy and Solvent on Rates. *J. Phys. Chem.* **1990**, *94*, 2889–2896.

(21) Burel, L.; Mostafavi, M.; Murata, S.; Tachiya, M. Transient Effect in Fluorescence Quenching by Electron Transfer. 4. Long-Range Electron Transfer in a Nonpolar Solvent. *J. Phys. Chem. A* **1999**, *103*, 5882–5888.

(22) Scully, A. D.; Ohtaka, H.; Takezaki, M.; Tominaga, T. Diffusion-Facilitated Direct Determination of Intrinsic Parameters for Rapid Photoinduced Bimolecular Electron-Transfer Reactions in Nonpolar Solvents. *J-. Phys. Chem. A* **2015**, *119*, 2770–2779.

(23) Liang, M.; Kaintz, A.; Baker, G. A.; Maroncelli, M. Bimolecular Electron Transfer in Ionic Liquids: Are Reaction Rates Anomalously High? *J. Phys. Chem. B* **2012**, *116*, 1370–1384.

(24) Nançoz, C.; Rumble, C.; Rosspeintner, A.; Vauthey, E. Bimolecular Photoinduced Electron Transfer in Non-Polar Solvents Beyond the Diffusion Limit. *J. Chem. Phys.* **2020**, *152*, 244501.

(25) de Rege, P. J. F.; Williams, S. A.; Therien, M. J. Direct Evaluation of Electronic Coupling Mediated by Hydrogen Bonds: Implications for Biological Electron Transfer. *Science* **1995**, *269*, 1409–1413.

(26) Ward, M. D. Photo-Induced Electron and Energy Transfer in Non-Covalently Bonded Supramolecular Assemblies. *Chem. Soc. Rev.* **1997**, *26*, 365–375.

(27) Sun, L.; Burkitt, M.; Tamm, M.; Raymond, M. K.; Abrahamsson, M.; LeGourriérec, D.; Frapart, Y.; Magnuson, A.; Kenéz, P. H.; Brandt, P. et al. Hydrogen-Bond Promoted Intramolecular Electron Transfer to Photogenerated Ru(III):A Functional Mimic of TyrosineZ and Histidine 190 in Photosystem II. *J. Am. Chem. Soc.* **1999**, *121*, 6834–6842.

(28) Piotrowiak, P. Photoinduced Electron Transfer in Molecular Systems: Recent Developments. *Chem. Soc. Rev.* **1999**, *28*, 143–150.

(29) Prasad, E.; Gopidas, K. R. Photoinduced Electron Transfer in Hydrogen Bonded Donor-Acceptor Systems. Study of the Dependence of Rate on Free Energy and Simultaneous Observation of the Marcus and Rehm-Weller Behaviors. *J. Am. Chem. Soc.* **2000**, *122*, 3191.

(30) Ghosh, H. N.; Adamczyk, K.; Verma, S.; Dreyer, J.; Nibbering, E. T. J. On the Role of Hydrogen Bonds in Photoinduced Electron-Transfer Dynamics between 9-Fluorenone and Amine Solvents. *Chem. - Eur. J.* **2012**, *18*, 4930–4937.

(31) Venkatraman, R. K.; Orr-Ewing, A. J. Solvent Effects on Ultrafast Photochemical Pathways. *Acc. Chem. Res.* **2021**, *54*, 4383–4394.

(32) Davis, M. M.; Helzer, H. B. Titrimetric and Equilibrium Studies Using Indicators Related to Nile Blue A. *Anal. Chem.* **1966**, *38*, 451–461.

(33) Moog, R. S.; Kim, D. D.; Oberle, J. J.; Ostrowski, S. G. Solvent Effects on Electronic Transitions of Highly Dipolar Dyes: Solvent Effects on Electronic Transitions of Highly Dipolar Dyes. *J. Phys. Chem. A* **2004**, *108*, 9294–9301.

(34) R. J. Cave, R. J.; Castner Jr, E. W. Time-Dependent DFT Investigation of the Ground and Excited States of Coumarins 102, 152, 153 and 343. *J. Phys. Chem. A* **2002**, *106*, 12117–12123.

(35) Letrun, R.; Vauthey, E. Excitation Wavelength Dependence of the Dynamics of Bimolecular Photoinduced Electron Transfer Reactions. *J. Phys. Chem. Lett.* **2014**, *5*, 1685–1690.

(36) Gardecki, J. A.; Maroncelli, M. Set of Secondary Emission Standard for Calibration of the Spectral Responsivity in Emission Spectroscopy. *Appl. Spectrosc.* **1998**, *52*, 1179–1189.

(37) Szakacs, Z.; Tasior, M.; Gryko, D.; Vauthey, E. Change of Quadrupole Moment upon Excitation and Symmetry Breaking in Multibranched Donor-Acceptor Dyes. *ChemPhysChem* **2020**, *21*, 1718–1730.

(38) Sajadi, M.; Quick, M.; Ernsting, N. P. Femtosecond Broadband Fluorescence Spectroscopy by Down- and Up-Conversion in β-Barium Borate Crystals. *Appl. Phys. Lett.* **2013**, *103*, 173514.

(39) Aster, A.; Licari, G.; Zinna, F.; Brun, E.; Kumpulainen, T.; Tajkhorshid, E.; Lacour, J.; Vauthey, E. Tuning Symmetry Breaking Charge Separation in Perylene Bichromophores by Conformational Control. *Chem. Sci.* **2019**, *10*, 10629–10639.

(40) Beckwith, J. S.; Aster, A.; Vauthey, E. The Excited-State Dynamics of the Radical Anions of Cyanoanthracenes. *Phys. Chem. Chem. Phys.* **2022**, *24*, 568–577.

(41) Abraham, M. J.; Murtola, T.; Schulz, R.; Pall, S.; Smith, J. C.; Hess, B.; Lindahl, E. GROMACS: High Performance Molecular Simulations through Multi-Level Parallelism from Laptops to Supercomputers. *SoftwareX* **2015**, *1-2*, 19–25.

(42) Jorgensen, W. L.; Maxwell, D. S.; Tirado-Rives, J. Development and Testing of the

OPLS All-Atom Force Field on Conformational Energetics and Properties of Organic Liquids. *J. Am. Chem. Soc.* **1996**, *118*, 11225–11236.

(43) Price, M. L. P.; Ostrovsky, D.; Jorgensen, W. L. Gas-Phase and Liquid-State Properties of Esters, Nitriles, and Nitro Compounds with the OPLS-AA Force Field. *J. Comput. Chem.* **2001**, *22*, 1340–1352.

(44) Sousa da Silva, A. W.; Vranken, W. F. ACPYPE - AnteChamber PYthon Parser InterfacE. *BMC Res. Notes* **2012**, *5*, 367.

(45) Lee, C.; Yang, W.; Parr, R. G. Development of the Colle-Salvetti Correlation-Energy Formula into a Functional of the Electron Density. *Phys. Rev. B* **1988**, *37*, 785–789.

(46) Frisch, M. J.; Trucks, G. W.; Schlegel, H. B.; Scuseria, G. E.; Robb, M. A.; Cheeseman, J. R.; Scalmani, G.; Barone, V.; Petersson, G. A.; Nakatsuji, H. et al. Gaussian 16 Rev. B.01. **2016**,

(47) Chirlian, L. E.; Francl, M. M. Atomic Charges Derived from Electrostatic Potentials: A Detailed study. *J. Comput. Chem.* **1987**, *8*, 894–905.

(48) Bernetti, M.; Bussi, G. Pressure Control Using Stochastic Cell Rescaling. *J. Chem. Phys.* **2020**, *153*, 114107.

(49) Hoover, W. G. Canonical Dynamics: Equilibrium Phase-Space Distributions. *Phys. Rev. A* **1985**, *31*.

(50) Nicolet, O.; Vauthey, E. Ultrafast Nonequilibrium Charge Recombination Dynamics of Excited Donor-Acceptor Complexes. *J. Phys. Chem. A* **2002**, *106*, 5553–5562.

(51) Moog, R. S.; Davis, W. W.; Ostrowski, S. G.; Wilson, G. L. Solvent Effects on Electronic Transitions in Several Coumarins. *Chem. Phys. Lett.* **1999**, *299*, 265–271.

(52) Shida, T. *Electronic Absorption Spectra of Radical Ions*; Elsevier: Amsterdam, 1988; Vol. 34.

(53) Angulo, G.; Rosspeintner, A.; Lang, B.; Vauthey, E. Optical Transient Absorption Experiments Reveal the Failure of Formal Kinetics in Diffusion Assisted Electron Transfer Reactions. *Phys. Chem. Chem. Phys.* **2018**, *20*, 25531 – 25546.

(54) van Stokkum, I. H. M.; Larsen, D. S.; van Grondelle, R. Global and Target Analysis of Time-Resolved Spectra. *Biochim. Biophys. Acta, Bioenerg.* **2004**, *1657*, 82–104.

(55) Beckwith, J. S.; Rumble, C. A.; Vauthey, E. Data Analysis in Transient Electronic Spectroscopy – an Experimentalist's View. *Int. Rev. Phys. Chem.* **2020**, *39*, 135–216.

(56) Pagès, S.; Lang, B.; Vauthey, E. Ultrafast Spectroscopic Investigation of the Charge Recombination Dynamics of Ion Pairs Formed Upon Highly Exergonic Bimolecular Electron Transfer Quenching: Looking for the Normal Region. *J. Phys. Chem. A* **2004**, *108*, 549–555.

(57) Mohammed, O. F.; Adamczyk, K.; Banerji, N.; Dreyer, J.; Lang, B.; Nibbering, E. T. J.; Vauthey, E. Direct Femtosecond Observation of Tight and Loose Ion Pairs upon Photoinduced Bimolecular Electron Transfer. *Angew. Chem. Int. Ed.* **2008**, *47*, 9044–9048.

(58) Rumble, C. A.; Vauthey, E. Molecular Dynamics Simulations of Bimolecular Electron Transfer: the Distance-Dependent Electronic Coupling. *J. Phys. Chem. B* **2021**, *125*, 10527–10537.

(59) Weller, A. Photoinduced Electron Transfer in Solutions: Exciplex and Radical Ion Pair Formation Free Enthalpies and their Solvent Dependence. *Z. Phys. Chem.* **1982**, *133*, 93–98.

(60) Asahi, T.; Ohkohchi, M.; Mataga, N. Energy Gap Dependences of Charge Recombination Processes of Ion Pairs Produced by Excitation of Charge Transfer Complexes: Solvent Polarity Effects. *J. Phys. Chem.* **1993**, *97*, 13132–13137.

(61) Chen, P.; Mecklenburg, S. L.; Meyer, T. J. Solvent and Temperature Dependence of Electron Transfer in the Inverted Region. *J. Phys. Chem.* **1993**, *97*, 13126–13131, doi: 10.1021/j100152a015.

(62) Castner Jr., E. W.; Kennedy, D.; Cave, R. J. Solvent as Electron Donor: Donor/Acceptor Electronic Coupling is a Dynamical Variable. *J. Phys. Chem. A* **2000**, *104*, 2869–2885.

(63) Morandeira, A.; Fürstenberg, A.; Gumy, J.-C.; Vauthey, E. Fluorescence Quenching in Electron Donating Solvents. 1. Influence of the Solute-Solvent Interactions on the Dynamics. *J. Phys. Chem. A* **2003**, *107*, 5375–5383.

(64) Young, H. D. *Statistical Treatment of Experimental Data*; McGraw-Hill: New York, 1962.

(65) Inakollu, V. S. S.; Geerke, D. P.; Rowley, C. N.; Yu, H. Polarisable Force Fields: What Do They Add in Biomolecular Simulations? *Curr. Opin. Struct. Biol.* **2020**, *61*, 182–190.

(66) Kikuchi, K. A New Aspect of Photoinduced Electron Transfer in Acetonitrile. *J. Photochem. Photobiol. A* **1992**, *65*, 149.

(67) Kuzmin, M. G. Exciplex Mechanism of Excited State Electron Transfer Reactions in Polar Media. *J. Photochem. Photobiol. A* **1996**, *102*, 51–57.

(68) Dossot, M.; Allonas, X.; Jacques, P. Singlet Exciplexes between a Thioxanthone Derivative and Substituted Aromatic Quenchers: Role of the Resonance Integral. *Chem. Eur. J.* **2005**, *11*, 1763–1770.

TOC Graphic

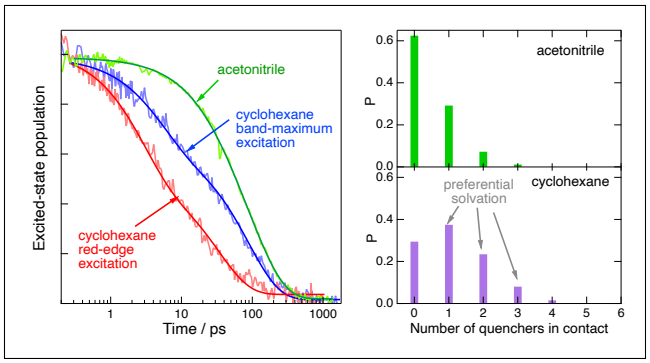
Excited-state population
acetonitrile
cyclohexane
band-maximum
excitation
cyclohexane
red-edge
excitation
1
10
100
1000
Time / ps
acetonitrile
P
0.6
0.4
0.2
0.0
preferential
solvation
cyclohexane
0
1
2
3
4
5
6
Number of quenchers in contact